Hindawi
Journal of Chemistry
Volume 2020, Article ID 8090846, 11 pages
https://doi.org/10.1155/2020/8090846

Research Article

Innovative Methodology for Sulfur Release from Copper Tailings by the Oxidation Roasting Process

Bing Luo,[1,2,3] Tongjiang Peng,[1,2,4] and Hongjuan Sun[1,2]

[1]*Key Laboratory of Ministry of Education for Solid Waste Treatment and Resource Recycle, Southwest University of Science and Technology, Mianyang, Sichuan 621010, China*
[2]*Institute of Mineral Materials and Applications, Southwest University of Science and Technology, Mianyang, Sichuan 621010, China*
[3]*City College, Southwest University of Science and Technology, Mianyang, Sichuan 621000, China*
[4]*Center of Forecasting and Analysis, Southwest University of Science and Technology, Mianyang, Sichuan 621010, China*

Correspondence should be addressed to Tongjiang Peng; tjpeng@swust.edu.cn and Hongjuan Sun; sunhongjuan@swust.edu.cn

Received 14 March 2020; Accepted 29 May 2020; Published 15 July 2020

Academic Editor: Sedat Yurdakal

To effectively prevent the accumulation of copper tailings from producing acid mine drainage (AMD) and maximize the comprehensive utilization of copper tailings, the process of oxidation roasting was adopted to release sulfur in the form of SO_2 to achieve the purpose of sulfur recovery later. Based on the AMD risk assessment, thermogravimetric (TG) analysis, and differential scanning calorimeter (DSC) analysis, the influences of roasting temperature, residence time, and air flow in the roasting process were investigated. The thermal stability, reaction equilibrium, mineral transformation, and residual S content were characterized by TG-DSC, HSC chemical software 6.0, X-ray diffraction (XRD), and combustion neutralization, respectively. The optimum conditions for sulfur release in the roasting process were shown with a temperature of 1200°C, a residence time of 60 min, and an air flow of 0.8 L/min. Under these conditions, the sulfur release rate was 99.82%, and the residual S content was 0.05%. Subsequently, the process of sulfur release was proposed as four steps: oxidative decomposition of pyrrhotite, formation of ferric sulfate, decomposition of ferric sulfate, and formation of hematite. All of the findings could propose a theoretical and experimental reference for the recovery of the sulfur component from tailings rich in sulfide minerals.

1. Introduction

Copper tailings are solid wastes which are discharged in slurry after processing including crushing, grinding, sorting, and extracting target components from copper ores under specific economic and technical conditions [1]. In China, for every ton of copper mine, approximately 400 tons tailings were dumped. Subsequently, a large amount of copper tailings was stored up, not only encroached on a large number of land resources but also posed serious threats to the environment and also caused serious waste of resources [2]. Especially, for the copper tailings which contained metallic sulfide, it was easy to produce AMD which caused severe environmental pollution [3, 4]. Meanwhile, sulfur in copper tailings also affected the grade of valuable metals extracted from copper tailings [5]. Additionally, it was possible for sulfur as a resource to be collected to make sulfuric acid which was the important application of sulfur [6, 7]. Therefore, it was necessary to release and recover sulfur from copper tailings. Innovative and cleaner methodology for recovery of S from copper tailings was increasingly needed to promote utilization of copper tailings more sustainable and respectful to ecological environment.

Generally, two methods to release sulfur from tailings rich in pyrite or pyrrhotite were involved, including flotation separation [8–10] and roasting [11]. The tailings rich in pyrrhotite had succeeded in desulfurization to less than 0.4 wt.% by optimizing the flotation process with respect to solution pH, activator, collector, frothier, and air-solid ratio [12]. Moreover, acid leaching and reverse flotation by using

mixing barrel, flotation column, and flotation machine had also reduced the sulfur content of pyrite from 0.5% to 0.01% [13]. However, in the process of flotation, tedious step with some chemical reagents which were easy to bring secondary pollution was involved. Compared with flotation, roasting was more suitable for release and recovery of sulfur, including reductive roasting, sulphation roasting, and oxidation roasting. When the temperature exceeded 1430°C, hydrogen, as a reducing agent, could combine with sulfur from the surface of pyrite to form hydrogen sulfide [14]. Pyrite could also be translated to ferric sulfate by sulphation process. With temperature ranging from 1000°C to 1350°C, the sulfur component diffused and was released in gaseous SO_x [15], where residual S in the roasted slag declined from 1.52% to 0.20% as a result of thermal decomposition of $FeSO_4$. Moreover, pyrrhotite was formed by desulfurization during the thermal decomposition of pyrite. In an aerobic or carbon dioxide atmosphere, pyrrhotite could be oxidized to form iron oxides and gaseous SO_x [16, 17]. When the concentration of SO_2 in gaseous SO_x reached or exceeded 3%, SO_2 could be collected together to produce sulfuric acid [18], and iron oxides could be recovered in subsequent processing. However, the change of the mineral phase, the release process, and mechanism of sulfur components during the roasting in the copper tailings had been rarely reported.

In this study, it involved resource utilization of sulfur from pyrrhotite in copper tailings. Based on the properties and AMD risks of copper tailings, oxidation roasting was proposed to release sulfur, and the sulfur release process, sulfur release rate, composition, and phase changes of the roasted slag were investigated. The objective of this research was to ascertain the sulfur release mechanism.

2. Experimental

2.1. Materials. The copper tailing samples (LW) used in this study were obtained from Liwu Copper, Sichuan, China. The collected samples were dried, crushed, and ground to 100 mesh. The samples were then mixed and stored for later use.

2.2. Experimental Procedure and Method

2.2.1. Chemical AMD Prediction Test. To evaluate the AMD risks of copper tailings piled effectively, the net acid generation (NAG) test, which involved several parameters, including sulfur content of copper tailings, acid neutralization capacity (ANC), net acid-producing potential (NAPP), and net acid generation (NAG) [4], was performed firstly.

The test of ANC was conducted as follows: 1 g ground sample was added to a 100 mL beaker containing 25 mL HCl (0.2 mol·L^{-1}) at 90°C for 3 h. After being cooled, it was titrated with NaOH (0.2 mol·L^{-1}) to pH 7, and the ANC was determined according to the following formula:

$$\mathrm{ANC} = (25 - V) \times 9.8, \tag{1}$$

where ANC is an index reflecting the sample's ability to neutralize acid by itself, kg H_2SO_4·t^{-1}, and V is the volume of NaOH used in the titration process, mL.

The NAPP was calculated as the following formula:

$$\mathrm{NAPP} = S \times 30.625 - \mathrm{ANC}, \tag{2}$$

where NAPP is a value which assessed the sample's net acid potential, kg H_2SO_4·t^{-1}, and S is the sulfur content of the copper tailings, %.

The test of NAG was conducted as follows: 2.5 g ground sample was added to a 500 ml conical flask containing 250 mL H_2O_2 (15%). After being left in the fume hood for 24 h, the mixture was boiled for about 1 h to remove remaining H_2O_2. Then, the mixture was cooled to room temperature, and it was titrated with NaOH (0.1 mol·L^{-1}) to pH 7, and the NAG was calculated as the following formula:

$$\mathrm{NAG} = 1.96 \times 10^3 \times V, \tag{3}$$

where NAG is a value of the sample's net acid generation, kg H_2SO_4·t^{-1}, and V is the volume of NaOH used in the titration process, mL.

$$\mathrm{APR} = \frac{\mathrm{ANC}}{(S \times 30.625)}, \tag{4}$$

where APR is the acid potential ratio and S is the sulfur content of the copper tailings, %.

2.2.2. Oxidation Roasting Test. Figure 1 shows the experiment equipment. The oxidation roasting test was carried out in a programmable energy-saving tubular furnace (LTKC-6-16A). From Figure 2, 20 ground samples (LW) were charged into a corundum crucible. Subsequently, the corundum crucible was put in a programmable energy-saving tubular furnace and heated at a temperature of 300°C–1200°C for a soaking time ranging from 20 min to 60 min. Meanwhile, the concentration of SO_2 was monitored at different temperatures in real time by a monitor of SO_2. SO_2 could be collected to produce sulfuric acid. During the oxidation roasting, the heating rate was 10°C/min under 1000°C, and the heating rate was 5°C/min above 1000°C. In addition, the effect of the filling rate (0 L/min, 0.2 L/min, 2.4 L/min, 0.6 L/min, 0.8 L/min, and 1.0 L/min) was also investigated. After the oxidation roasting, the roasted slag was made natural cooling to room temperature, and then it was removed from the tubular furnace for further analysis.

The content of residual S in the copper slag was determined by the combustion neutralization method [19], and the sulfur release rate (n) was calculated as the following formula:

$$n = \left(1 - \frac{M_2 S_2}{M_1 S_1}\right) \times 100\%, \tag{5}$$

where M_1 and M_2 are the masses of samples before and after roasting, respectively, g and S_1 is the initial sulfur content of the copper tailings, while S_2 represents the residual sulfur content of the roasted slag, %.

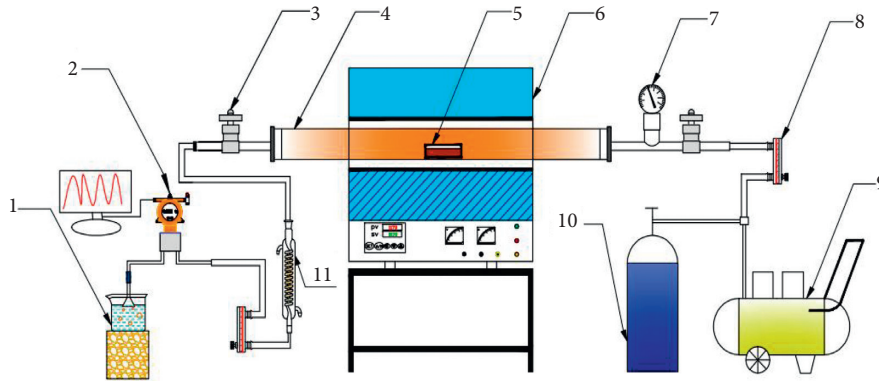

Figure 1: Experiment equipment for oxidation roasting: (1) absorption liquid, (2) monitor of SO_2, (3) flow control device, (4) furnace tube, (5) alumina crucible, (6) tube furnace, (7) pressure gage, (8) flow meter, (9) air blower, (10) nitrogen cylinder, and (11) condenser pipe.

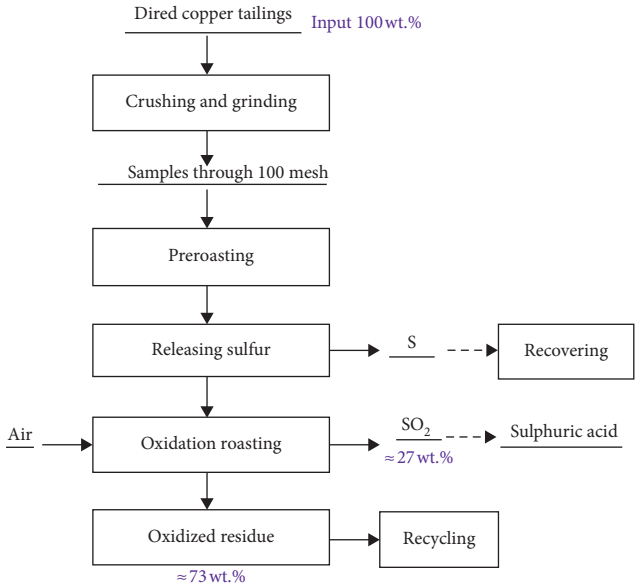

Figure 2: Experiment process of sulfur release from copper tailings (LW).

2.3. Analytical Methods. In this study, the mineralogical phase compositions of both raw tailings and roasted samples were tested by X-ray diffraction (XRD, X'Pert pro +3 KW, Netherlands), using Cu Kα radiation with a continuous scanning step of 0.02° in 2θ ranging from 3° to 80°. Subsequently, software X'Pert HighScore Plus was used for analyzing the diffraction patterns of XRD.

The sulfur content of both raw tailings and roasted samples was determined using the combustion neutralization method. Moreover, the concentration of SO_2 in the roasting process was obtained continuously by a SO_2 monitor (SK-600) made in China.

Apart from sulfur, the contents of other chemical compositions in raw tailings were identified by the X-ray fluorescence spectrometer (XRF, Axios, Netherlands).

Thermogravimetry and differential scanning calorimetry analysis (TG-DSC) was observed by a thermal analyzer (NETZSCH STA 449F5) in the air atmosphere, heated from room temperature to 1500°C with a heating rate of 10°C min^{-1}.

In addition, HSC Chemistry Software 6.0 was used to work out basic thermodynamic calculations including the standard free energy (ΔG^{θ}). These calculations were employed to evaluate the possible reaction and explain the mechanism of sulfur release during oxidation roasting.

3. Results and Discussion

3.1. Characteristics and AMD Risk Assessment of Copper Tailings. Table 1 shows chemical compositions of copper tailings, and Figure 3 shows phase compositions of the copper tailings. From Figure 3, the main mineral in the copper tailings was quartz, biotite, clinochlore, pyrrhotite, lepidocrocite, and sulfur. Therefore, the sulfur minerals in copper tailings, including pyrrhotite and natural sulfur, could be released by oxidative roasting.

Table 2 shows the chemical AMD prediction test results for the copper tailings. pH of the sample (LW) was 6.32, so both of solid phase solubility and the salt content would gradually increase. Then, it was qualified to produce AMD [20]. At the same time, the content of sulfur in the sample (LW) was relatively high. With oxygen and water, it was easy to form AMD due to the oxidation of sulfide minerals. From Table 2, ANC was smaller than NAPP and NAG, indicating that the copper tailings themselves could not effectively neutralize the acid generated by the oxidation of sulfide in some parts, which was exactly explained by the positive NAPP [21]. On the basis of classifications listed in Table 2, with NAPP > 20 and APR < 1, AMD was formed easily in the copper tailings by oxidation of sulfide minerals, and AMD was considered a delayed (chemical time bomb) and persistent geochemical disaster [22]. Therefore, to remove or recover sulfur from the copper tailings was of great importance to not only control tailing pollution but also to realize recycling and utilization of the resource.

3.2. Phase Transformation, Thermal Effect, and Decomposition Kinetics

3.2.1. Phase Transformation of the Roasted Slag. Figure 4 shows the XRD patterns of the roasted slag at different roasting temperatures. When the temperature was 300°C,

Table 1: Chemical composition of the copper tailings (wt. %).

Components	Fe_2O_3	SO_3	SiO_2	Al_2O_3	Na_2O	ZnO	CaO	K_2O	MgO	TiO_2	CuO	P_2O_5	Co_3O_4	PbO	ZrO_2	MnO	SrO	Total
Content	36.35	27.82	22.81	6.03	2.12	1.61	1.16	0.93	0.47	0.25	0.22	0.10	0.05	0.03	0.02	0.02	0.01	100%

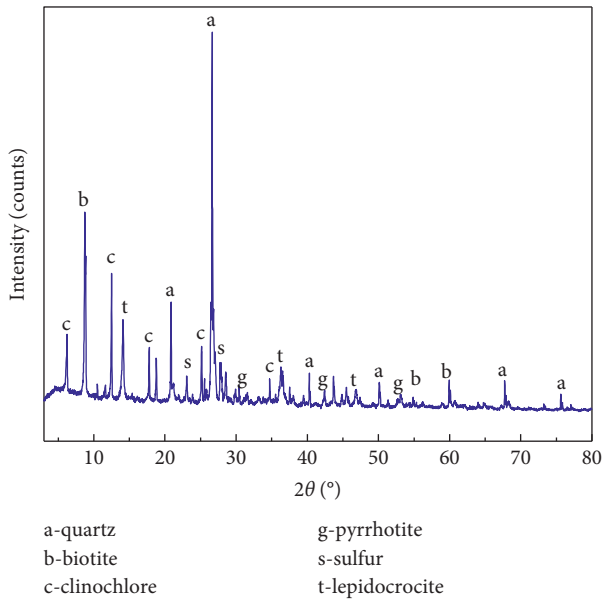

Figure 3: XRD spectra of the copper tailing sample (LW).

the main phase of the roasting slag was quartz, biotite, pyrrhotite, and chlorite, indicating that no thermal decomposition reaction occurred. Compared with the raw material, the pattern of lepidocrocite and natural sulfur disappeared. With the increasing temperature, some pyrrhotite decomposed to form FeS and S. Subsequently, FeS was oxidized to form $FeSO_4$ and Fe_2O_3. When the temperature reached 600°C, quartz, biotite, clinochlore, pyrrhotite, and hematite existed in the roasted slag. However, the peak strength of clinochlore and pyrrhotite was reduced to a certain level, and a new phase ($FeSO_4$) was present. As the temperature continued to rise, $FeSO_4$ began to decompose to hematite and SO_2. At 900°C, the main phases in the roasted slag were quartz and biotite, and hematite and anorthite formed. At 1100°C, the phase of the roasted slag did not change in kind, but the peak strength of biotite decreased gradually. Under the optimal roasting temperature of 1200°C, the main phases in the roasting slag were quartz, hematite, and anorthite.

3.2.2. Thermal Effect Change. In order to confirm the characteristics of the copper tailings during oxidation roasting and explain the path of the sulfur liberation reaction of pyrrhotite indirectly, the TG-DSC curves of copper tailings (LW) are performed in Figure 5. On the TG curve, the weight loss was about 6.48% from room temperature to 344°C, where the weight loss was about 0.72% as a result of loss of adsorbed water from room temperature to 110°C. From 110°C to 344°C, a small amount of natural sulfur sublimates emerged, and lepidocrocite lost crystallization water, with a weight loss of about 5.76%. Over the temperature range of 344°C–428°C, the mass of samples increased about 0.59%, which was related to the formation of $FeSO_4$ and Fe_2O_3 from the oxidation decomposition of pyrrhotite [23, 24]. The weight loss between 428°C and 600°C was 1.43%, which was in relation to the loss of interlayer structure water (528°C±) of clinochlore and sulfur release in pyrrhotite decomposition (550°C±) [25]. In the range of 600°C–900°C, $FeSO_4$, which was formed by the decomposition and oxidation of pyrrhotite, was further decomposed to release SO_2, with a weight loss of 1.75%. Then, an obvious mass loss (13.81%) from 900°C to 1200°C was presented in relation to the removal of structural water from biotite and the loss of sulfur in the residual structure.

On the DSC curve, two endothermic peaks (251.8°C and 271.9°C) appeared, which corresponded to the endothermic effect, including desorption of crystallization water of lepidocrocite and phase change of pyrrhotite. The exothermic peaks (1003.8°C and 1155.3°C) were caused by the crystallization exothermic effects of calcium feldspar and hematite, respectively.

3.2.3. Thermodynamic Analysis. Under the condition of air, pyrrhotite was oxidized and decomposed to form SO_2. The possible reactions involved during oxidation roasting of copper tailings are listed as follows:

$$4Fe_{1-x}S(s) + 7O_2(g) = 2(1-x)Fe_2O_3(s) + 4SO_2(g) \quad (6)$$

$$3Fe_{1-x}S(s) + 5.5O_2(g) = (1-x)Fe_2O_3(s) + (1-x)FeSO_4(s) + 2SO_2(g) \quad (7)$$

$$2FeSO_4(s) = Fe_2O_3(s) + 2SO_2(g) + 0.5O_2(g) \quad (8)$$

$$S_2(g) + 2O_2(g) = 2SO_2(g) \quad (9)$$

Figure 6 shows the standard free energy (ΔG^θ) changes for equations (6)–(9) over the temperature ranging from 0°C to 1250°C. ΔG^θ for equations (6), (7), and (9) was negative over the temperature ranging from 0°C to 1200°C, suggesting these reactions were possible from the view of thermodynamics. Moreover, ΔG^θ for equation (8) became smaller with the increasing temperature, even became negative after 720°C, indicating that $FeSO_4$ could be decomposed to metal oxides and SO_2.

Take equation (6) for example:

$$\Delta G^\theta = 0.559T - 2290.1\left(\text{kJ}\cdot\text{mol}^{-1}\right). \quad (10)$$

Meanwhile, ΔG^θ could also be expressed as follows:

$$\Delta G^\theta = -\ln K^\theta, \quad (11)$$

Table 2: Acid-producing potential of the copper tailings.

Experimental parameter	Result	Classification	Category
pH	6.32		
EC (ds m^{-1})	1105		
ANC ($kgH_2SO_4.t^{-1}$)	88.2		Potentially acid-generating
NAPP ($kgH_2SO_4.t^{-1}$)	634.43	>20	
NAG ($kgH_2SO_4.t^{-1}$)	217.56		
APR	0.255	<1	

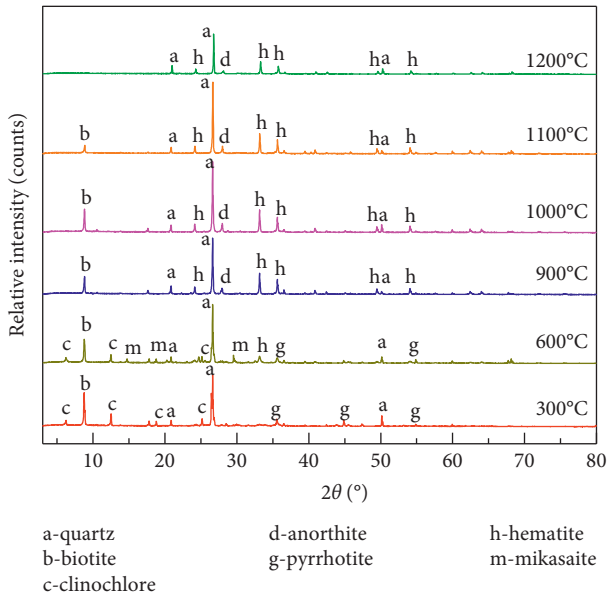

Figure 4: The XRD patterns of the roasted slag at varying temperature.

where K^{θ} is the equilibrium constant. K^{θ} is shown as

$$K^{\theta} = \frac{a^2_{Fe_2O_3} \times P^4_{SO_2}}{a^4_{FeS} \times P^7_{O_2}}. \quad (12)$$

Through equations (10)–(12),

$$a^2_{Fe_2O_3} = a^4_{FeS} \times e^{-\Delta G^{\theta}} \times \frac{P^7_{O_2}}{P_{SO_2}}, \quad (13)$$

where $a_{Fe_2O_3}$ is the activity of Fe_3O_4 in the roasted slag; a_{FeS} is the activity of FeS in the roasted slag; P_{SO2} is the partial pressure of SO_2 generated during the oxidation roasting; and P_{O2} is the partial pressure of O_2 present during the oxidation roasting.

When the thermodynamic temperature T, P_{O2}, P_{SO2} was determined, the relationship between $a_{Fe_2O_3}$ and a_{FeS} could be expressed correctly by equations (10)–(13) and could be calculated by equation (13), where the parabolic relationship between $a_{Fe_2O_3}$ and a_{FeS} was observed. In the case where the temperature was 1000°C and P_{SO2} was 1 atm simultaneously, the value of $e^{-G^{\theta}}$ and $1/P_{SO_2}$ was constant. Then, equation (13) turned into equation (14), and the results are present in Figure 7.

$$a_{Fe_2O_3} = t^{1/2} \times P^{7/2}_{O_2} \times a^2_{FeS}, \quad (14)$$

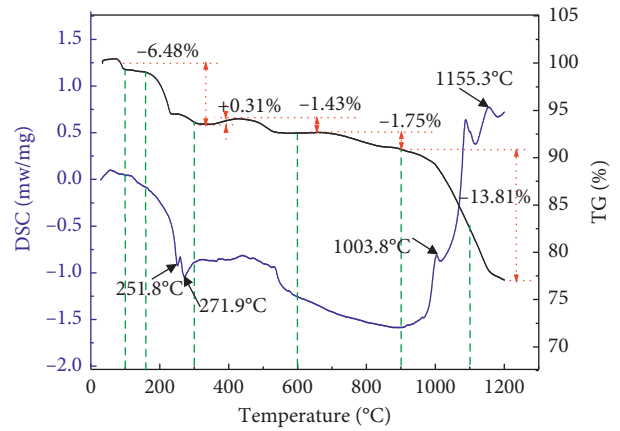

Figure 5: TG and DSC curves for copper tailings heated at 10°C min^{-1} in air.

where t is the constant, and $t = e^{-\Delta G^{\theta}} \times (1/P_{SO_2})$.

As shown in Figure 7, it was indicated that, with an increase in P_{O2}, $a_{Fe_2O_3}$ increased rapidly, which meant FeS was oxidized to Fe_2O_3 and SO_2, respectively. As a consequence, oxygen added in roasting could promote sulfur release.

3.3. Sulfur Release Rate and Residual S Content during Oxidation Roasting

3.3.1. Effect of the Roasting Temperature. The effect of roasting temperature on sulfur release rate and residual S content was investigated with temperature ranging from 300°C to 1200°C over a roasting time of 30 min at an air flow = 1.0 L/min. The results are presented in Figure 8. As illustrated in Figure 6, with an increase in the roasting temperature which was beneficial to thermal decomposition of sulfide minerals, the sulfur release rate and the residual S content were observed from 13.60% to 99.45% and from 23.70% to 0.15%, respectively. Corresponding to the above thermal analysis, it released sulfur vapor slowly before 600°C on account of pyrrhotite considered as solid solution which caused the sulfur to leave the particle very slowly. Moreover, sulfur began to be released as SO_2 at 600°C [15]. When the temperature further increased, the sulfur vapor diffused through the Fe_{1-x} S layer quickly and could combine with oxygen to form SO_2. However, the sulfur release rate and the residual S content were steady at 1200°C, indicating that a roasting temperature of 1200°C was recommended for the following tests.

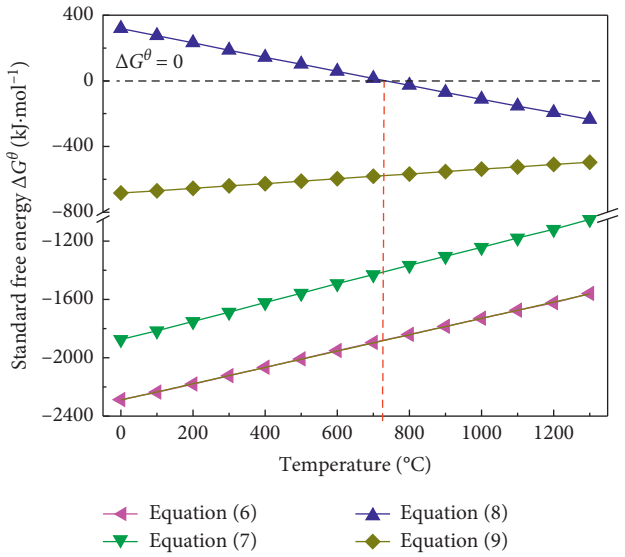

Figure 6: Standard free energy changes for reactions vs. temperature for equations (7)–(10).

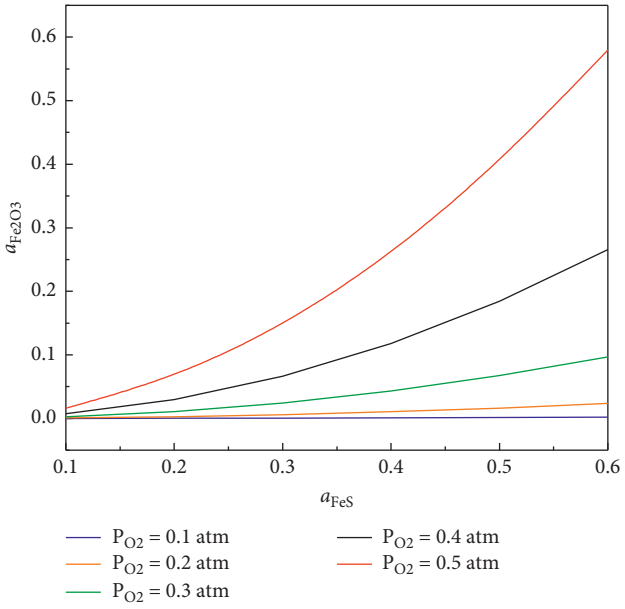

Figure 7: The relative relationship between $a_{Fe_2O_3}$ and a_{FeS}.

3.3.2. Effect of Residence Time. Figure 9 shows the effect of residence time on sulfur release rate and residual S content. From Figure 9, by increasing the duration time from 20 min to 60 min, the sulfur release rate and the residual S content were observed from 96.32% to 99.78% and from 1.01% to 0.06%, respectively. When the duration time was over 60 min, the sample could be roasted excessively to form the liquid phase, which prevented SO_2 from escaping in the oxidation process [26, 27]. Hence, the optimal duration was determined as 60 min to ensure proper sulfur fugacity.

3.3.3. Effect of Air Flow. The influence of air flow on sulfur release rate and residual S content is illustrated in Figure 10, indicating that, with an increase in an air flow from

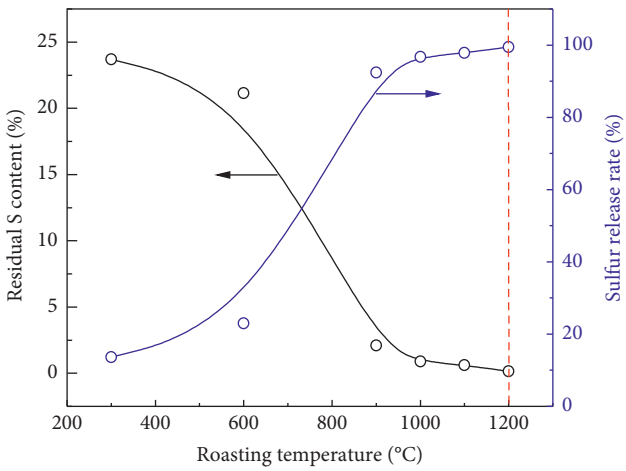

Figure 8: Effect of roasting temperature on sulfur release rate and residual S content (conditions: roasting time = 30 min and air flow = 1.0 L/min).

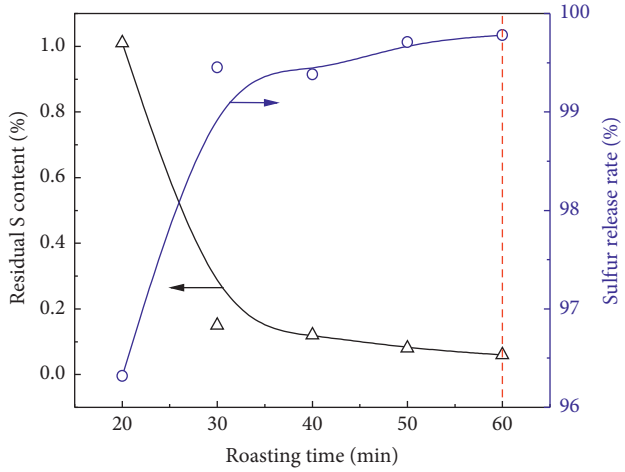

Figure 9: Effect of residence time on sulfur release rate and residual S content (conditions: roasting temperature = 1200°C and air flow = 1.0 L/min).

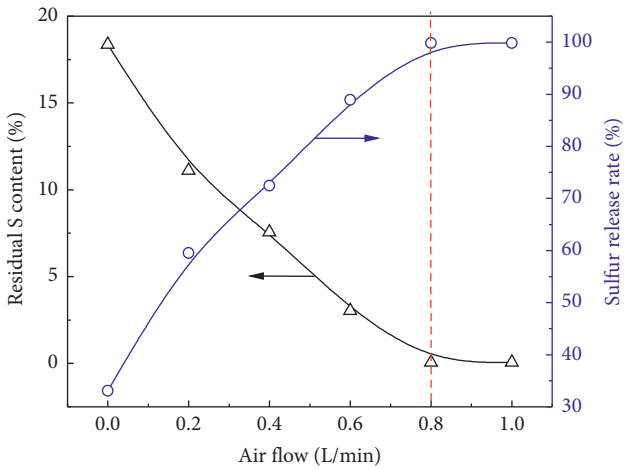

Figure 10: Effect of air flow on sulfur release rate and residual S content (conditions: roasting temperature = 1200°C and residence time = 60 min).

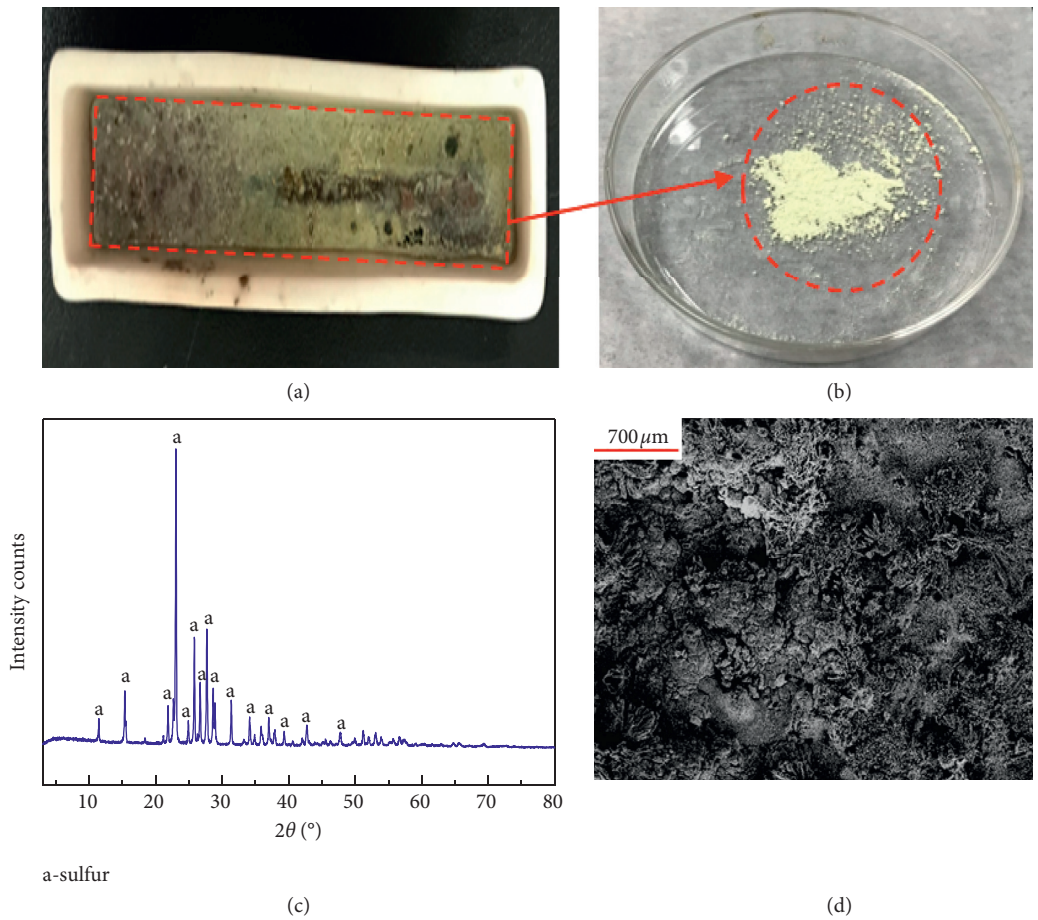

Figure 11: The photo of the (a) overall sample and (b) topmost sample roasted under anoxic conditions at 1200°C for 40 min; (c) the XRD patterns and (d) SEM image of the top layer of the sample roasted.

0 L/min to 1 L/min, the sulfur release rate and the residual S content were observed from 59.53% to 99.82% and from 11.10% to 0.05%, respectively. When the sample weight was fixed, oxygen as a reactant not only affected the concentration of SO_2 but also played an important part in the reaction. With an increase in the air flow, the sulfur release rate and the residual S content gradually became steady. Therefore, an optimum air flow was selected as 0.8 L/min.

Surprisingly, when air flow was 0 L/min, sulfur in the sample was released as sulfur vapor rather than SO_2. The results are observed in Figures 11(a) and 11(b). It was suggested that pyrrhotite lost sulfur firstly and the sulfur vapor diffused upward. Then, sulfur vapor was cooled and was deposited on the top layer of the sample. In order to confirm the yellow material deposited on the surface of the sample, the XRD was analyzed as shown in Figure 11(c). From Figure 11(c), the yellow material on the layer of the sample was S ($d_{222} = 3.8540$ Å, $d_{206} = 3.2190$ Å, and $d_{026} = 3.4470$ Å). Moreover, the SEM image of S is illustrated in Figure 11(d) which showed that the yellow powder had a fluffy structure.

3.4. Characterization of SO_2 Released and Roasted Slag

3.4.1. The Concentration of SO_2 Varying with Increasing Temperature. The release pattern of SO_2 is presented in Figure 12. From Figure 12, the presence of SO_2 began when the temperature arrived 600°C, and it reached the maximum concentration when the temperature was 1168°C. Interestingly, the distribution of SO_2 concentration was parabolic, and the concentration of SO_2 in the flue gas was 0~8.26%. Hence, SO_2 could be collected for sulfuric acid production through purification of SO_2, conversion of SO_2, and absorption of SO_3 when it met the requirements that the concentration of SO_2 in the gas reached 3% [28, 29].

3.4.2. The Characterization of the Roasted Slag. The chemical composition of the roasted slag is shown in Table 3. Compared with raw materials, more Fe_2O_3 and SiO_2 in the roasted slag existed. After sulfur was released in the form of SO_2, the total mass of the sample decreased, and the percentage of Fe_2O_3 increased obviously. Moreover, the residual S content of the tailings was 0.05%. According to the quality requirement of the ore suitable for steelmaking, the tailings with more than 55% TFe and with less than 1% S could be used in iron smelting [25].

Table 3: Chemical composition of the roasted slag (wt. %).

Components	Fe_2O_3	SO_3	SiO_2	Al_2O_3	Na_2O	ZnO	CaO	K_2O	BaO	MgO	TiO_2	CuO	P_2O_5	Co_3O_4	PbO	ZrO_2	MnO	SrO	Rb_2O	Total
Content	59.48	0.05	29.66	3.69	0.11	3.02	1.14	0.90	0.05	0.64	0.32	0.54	0.14	0.11	0.05	0.03	0.04	0.02	0.01	100%

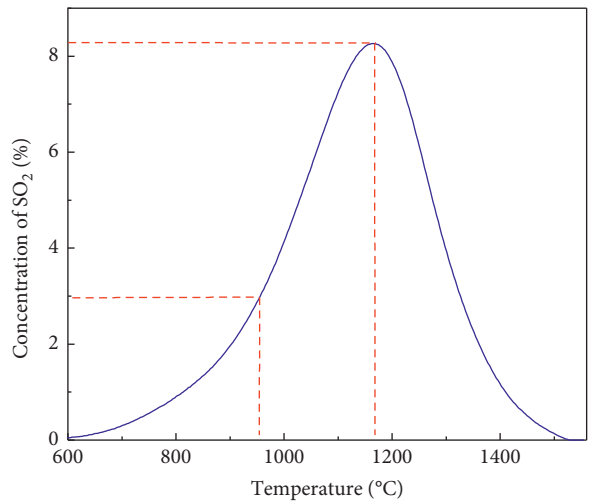

Figure 12: The release pattern of SO_2 during oxidation roasting.

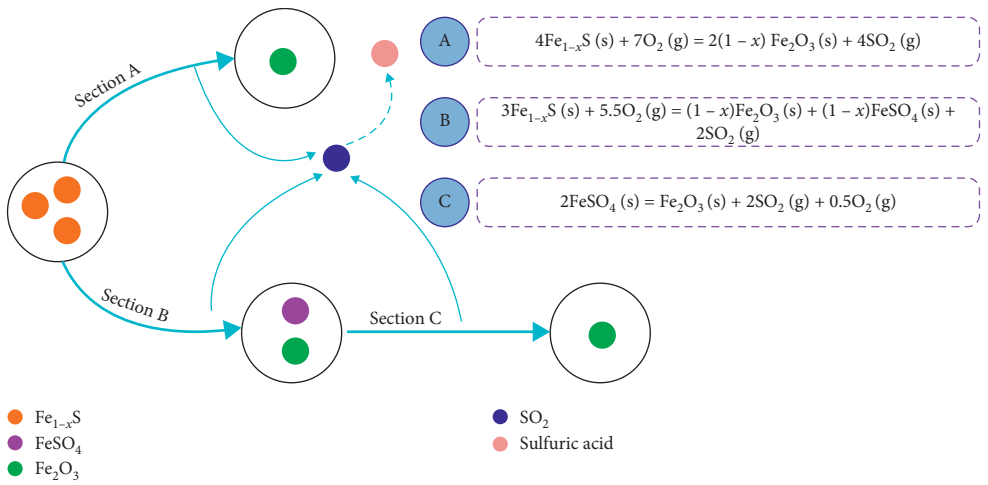

Figure 13: Schematic of the mechanism of sulfur release and phase transition.

3.5. Sulfur Release Mechanism and Phase Transition of Pyrrhotite. Based on the previous discussion, the mechanism of sulfur release from pyrrhotite could be proposed in Figure 13. The possible process is shown in the following four steps: the oxidation decomposition of pyrrhotite, the formation of ferric sulfate, the decomposition of ferric sulfate, and the formation of hematite. During roasting, SO_2 was partly released after oxidation decomposition of pyrrhotite, and the sulfur release rate increased with the increase of temperature. Under the condition of sufficient air, pyrrhotite was directly oxidized to hematite when it was heated. With air supplied insufficiently, pyrrhotite was partially oxidized to hematite and partially oxidized to ferric sulfate. Then, ferric sulfate was dissolved into hematite at higher temperatures. In the oxidation process of pyrrhotite, sulfur from the middle layer to the surface was oxidized and was escaped as SO_2, while hematite was formed in situ. The oxidation process of pyrrhotite was carried out from the surface layer to the inner layer with the increase of temperature and time. Finally, pyrrhotite was completely oxidized and decomposed, and hematite was generated in the roasted slag which could be used for iron recovery in the next step.

4. Conclusion

In this study, an innovative method was developed for release of S from copper tailings. The main findings from this work are concluded as follows:

(1) The main metal sulfide mineral in the copper tailings was pyrrhotite. The contents of Fe-total and S-total reached 36.35% and 27.82%, respectively. Therefore, S and Fe could be separated and recovered step by step successively where S release was necessary and was realized by oxidation roasting firstly.

(2) The AMD risk assessment showed that the copper tailings had acid-generating potential, and the NAPP was tested as 634.43 kg H_2SO_4 t^{-1}. The AMD would pose a severe threat to human health and ecological environment.

(3) The optimum conditions for sulfur release were obtained with a temperature of 1200°C, a residence time of 60 min, and an air flow of 0.8 L/min. Under these conditions, the sulfur release rate and the residual S content were 99.82% and 0.05%, respectively.

(4) In the process of oxidizing roasting, pyrrhotite was oxidized and decomposed to form ferric sulfate, hematite, and sulfur dioxide. With the increasing temperature and time, ferric sulfate decomposed to hematite and SO_2.

(5) The concentration of SO_2 released exceeds 3% and could meet the requirements of sulfuric acid production. Moreover, hematite with magnetic properties and quartz mainly existed in the roasted slag, suggesting that hematite could be separated and recovered by magnetic separation in the next step.

Data Availability

The data included the chemical composition of the tailings, the content of sulfur in the tailings, and the phases of the tailings under different conditions. Moreover, all data graphs in the manuscript were drawn with Origin software, and the original format of the graph was retained in the text.

Conflicts of Interest

The authors declare that they have no conflicts of interest.

Acknowledgments

The authors would like to express their sincere thanks to the Longshan Academic Research Support Program (no. 14tdgk02) and the Project of Key Research Platform Focused on Teachers' Research Innovation Team (no. 17LZXT11) both from Southwest University of Science and Technology of China.

References

[1] C. Geng, H.-J. Wang, W.-T. Hu, L. Li, and C.-S. Shi, "Recovery of iron and copper from copper tailings by coal-based direct reduction and magnetic separation," *Journal of Iron and Steel Research International*, vol. 24, no. 10, pp. 991–997, 2017.

[2] Y. Liu and L. Huang, "Magnetite recovery from copper tailings increases arsenic distribution in solution phase and uptake in native grass," *Journal of Environmental Management*, vol. 186, pp. 175–182, 2017.

[3] A. Manceau, M. Merkulova, M. Murdzek et al., "Chemical forms of mercury in pyrite: implications for predicting mercury releases in acid mine drainage settings," *Environmental Science & Technology*, vol. 52, no. 18, pp. 10286–10296, 2018.

[4] Y. Nleya, G. S. Simate, and S. Ndlovu, "Sustainability assessment of the recovery and utilisation of acid from acid mine drainage," *Journal of Cleaner Production*, vol. 113, pp. 17–27, 2016.

[5] Z. Luo, Y. Liu, R. L. Zhu, and X. Hu, "Inhibition of microbial pyrite oxidation by PropS-SH for the control of acid mine drainage," *International Journal of Electrochemical Science*, vol. 11, pp. 6501–6513, 2016.

[6] B. S. Maluckov and M. N. Mitrić, "Electrochemical behavior of pyrite in sulfuric acid in presence of amino acids belonging to the amino acid sequence of rusticyanin," *Bioelectrochemistry*, vol. 123, pp. 112–118, 2018.

[7] C. Yang, Y. Chen, P. A. Peng, C. Li, X. Chang, and Y. Wu, "Trace element transformations and partitioning during the roasting of pyrite ores in the sulfuric acid industry," *Journal of Hazardous Materials*, vol. 167, no. 1–3, pp. 835–845, 2009.

[8] R. Alam and J. Q. Shang, "Effect of operating parameters on desulphurization of mine tailings by froth flotation," *Journal of Environmental Management*, vol. 97, pp. 122–130, 2012.

[9] T. Nuorivaara, A. Björkqvist, J. Bacher, and R. Serna-Guerrero, "Environmental remediation of sulfidic tailings with froth flotation: reducing the consumption of additional resources by optimization of conditioning parameters and water recycling," *Journal of Environmental Management*, vol. 236, pp. 125–133, 2019.

[10] J. Rincon, S. Gaydardzhiev, and L. Stamenov, "Investigation on the flotation recovery of copper sulphosalts through an integrated mineralogical approach," *Minerals Engineering*, vol. 130, pp. 36–47, 2019.

[11] Z. Xi, Z. Wang, X. Li, H. Guo, G. Yan, and J. Wang, "Improving the desulfurization degree of high-grade nickel matte via a two-step oxidation roasting process," *Metallurgical and Materials Transactions B*, vol. 49, no. 4, pp. 1834–1840, 2018.

[12] M. Benzaazoua, H. Bouzahzah, Y. Taha et al., "Integrated environmental management of pyrrhotite tailings at raglan mine: part 1 challenges of desulphurization process and reactivity prediction," *Journal of Cleaner Production*, vol. 162, pp. 86–95, 2017.

[13] H. Liu, S. A. Khoso, W. Sun et al., "A novel method for desulfurization and purification of fluorite concentrate using acid leaching and reverse flotation of sulfide," *Journal of Cleaner Production*, vol. 209, pp. 1006–1015, 2019.

[14] J. M. Lambert, G. Simkovich, and P. L. Walker, "The kinetics and mechanism of the pyrite-to-pyrrhotite transformation," *Metallurgical and Materials Transactions B*, vol. 29, no. 2, pp. 385–396, 1998.

[15] D. Zhu, C. Yang, J. Pan, Z. Guo, and S. Li, "New pyrometallurgical route for separation and recovery of Fe, Zn, In, Ga and S from jarosite residues," *Journal of Cleaner Production*, vol. 205, pp. 781–788, 2018.

[16] W. Lv, D. Yu, J. Wu, X. Yu, Y. Du, and M. Xu, "A mechanistic study of the effects of CO_2 on pyrrhotite oxidation," *Proceedings of the Combustion Institute*, vol. 36, no. 3, pp. 3925–3931, 2017.

[17] M. C. Mayoral, J. M. Andrés, M. T. Izquierdo, and B. Rubio, "Pyrrhotite deposition through thermal projection to simulate iron sulphide slagging in oxyfuel combustion," *Fuel*, vol. 101, pp. 197–204, 2012.

[18] C. Lei, B. Yan, T. Chen, S.-X. Quan, and X.-M. Xiao, "Comprehensive utilization of lead-zinc tailings, part 1: pollution characteristics and resource recovery of sulfur," *Journal of Environmental Chemical Engineering*, vol. 3, no. 2, pp. 862–869, 2015.

[19] M. J. F. Llorente and J. E. C. García, "Suitability of thermochemical corrections for determining gross calorific value in biomass," *Thermochimica Acta*, vol. 468, no. 1-2, pp. 101–107, 2008.

[20] Y. Ouyang, Y. Liu, R. Zhu et al., "Pyrite oxidation inhibition by organosilane coatings for acid mine drainage control," *Minerals Engineering*, vol. 72, pp. 57–64, 2015.

[21] Y. Liu, X. Hu, and Y. Xu, "PropS-SH/SiO_2 nanocomposite coatings for pyrite oxidation inhibition to control acid mine drainage at the source," *Journal of Hazardous Materials*, vol. 338, pp. 313–322, 2017.

[22] A.-M. P. Louis, H. Yu, S. L. Shumlas, B. V. Aken, M. A. A. Schoonen, and D. R. Strongin, "Effect of phospholipid on pyrite oxidation and microbial communities under simulated acid mine drainage (AMD) conditions," *Environmental Science & Technology*, vol. 49, no. 13, pp. 7701–7708, 2015.

[23] N. Belzile, Y.-W. Chen, M.-F. Cai, and Y. Li, "A review on pyrrhotite oxidation," *Journal of Geochemical Exploration*, vol. 84, no. 2, pp. 65–76, 2004.

[24] M. J. Mengason, P. A. Candela, and P. M. Piccoli, "Molybdenum, tungsten and manganese partitioning in the system pyrrhotite-Fe-S-O melt-rhyolite melt: impact of sulfide segregation on arc magma evolution," *Geochimica et Cosmochimica Acta*, vol. 75, no. 22, pp. 7018–7030, 2011.

[25] C. M. V. B. Almeida and B. F. Giannetti, "The electrochemical behavior of pyrite-pyrrhotite mixtures," *Journal of Electroanalytical Chemistry*, vol. 553, pp. 27–34, 2003.

[26] K.-S. Lee, J.-H. Jung, S.-I. Keel, H.-K. Lee, and S.-S. Kim, "Characteristics of $CaCO_3$ Sorbent particles for the in-furnace desulfurization," *Transactions of the Korean Society of Mechanical Engineers B*, vol. 34, no. 2, pp. 121–127, 2010.

[27] D. Zhang, H. Tao, C. Yao, and Z. Sun, "Effects of residence time on the efficiency of desulfurization and denitrification in the bubbling reactor," *Chemical Engineering Science*, vol. 174, pp. 203–221, 2017.

[28] A. A. Kiss, C. S. Bildea, and P. J. T. Verheijen, "Optimization studies in sulfuric acid production," *Computer Aided Chemical Engineering*, vol. 21, pp. 737–742, 2006.

[29] M. L. S. Oliveira, C. R. Ward, M. Izquierdo et al., "Chemical composition and minerals in pyrite ash of an abandoned sulphuric acid production plant," *Science of the Total Environment*, vol. 430, pp. 34–47, 2012.